



HAL
open science

Effect of UVC pre-irradiation on the Suwannee river Natural Organic Matter (SRNOM) photooxidant properties

Davide Palma, Amina Khaled, Mohamad Sleiman, Guillaume Voyard, Claire
Richard

► **To cite this version:**

Davide Palma, Amina Khaled, Mohamad Sleiman, Guillaume Voyard, Claire Richard. Effect of UVC pre-irradiation on the Suwannee river Natural Organic Matter (SRNOM) photooxidant properties. Water Research, 2021, 202, pp.117395. 10.1016/j.watres.2021.117395 . hal-03292331

HAL Id: hal-03292331

<https://hal.science/hal-03292331>

Submitted on 20 Jul 2021

HAL is a multi-disciplinary open access archive for the deposit and dissemination of scientific research documents, whether they are published or not. The documents may come from teaching and research institutions in France or abroad, or from public or private research centers.

L'archive ouverte pluridisciplinaire **HAL**, est destinée au dépôt et à la diffusion de documents scientifiques de niveau recherche, publiés ou non, émanant des établissements d'enseignement et de recherche français ou étrangers, des laboratoires publics ou privés.

1 **Effect of UVC pre-irradiation on the Suwannee river Natural Organic Matter (SRNOM)**
2 **photooxidant properties**

3

4 Davide Palma, Amina Khaled, Mohamad Sleiman, Guillaume Voyard, Claire Richard*

5

6 Université Clermont Auvergne, CNRS, SIGMA-Clermont, ICCF, F-63000 Clermont-Ferrand, France

7

8

9 * : corresponding author

10 Email : claire.richard@uca.fr

11 Tel : +33 (0)4 73 40 71 42

12 Fax : +33 (0)4 73 40 77 00

13

14

15 **Abstract :** The present study aimed to investigate the changes in the chemical composition,
16 and in the optical and photooxidant properties of Suwannee River Natural Organic Matter
17 (SRNOM) induced by UVC (254 nm) treatment. The extent of the photodegradation was first
18 assessed by UV-visible/fluorescence spectroscopies and organic carbon analysis. An in-depth
19 investigation of the chemical changes was also conducted using liquid chromatography-mass
20 spectrometry and gas chromatography-mass spectrometry after derivatizations. A series of
21 mono, di and tricarbonyls and mono and dicarboxylic acids in C₁-C₆ were identified in
22 samples irradiated from 1 to 4 h. After 3 h of irradiation, carbonyls accounted for 46% of the
23 organic carbon remaining in solution whereas carboxylic acids represented about 2%. Then,
24 we investigated the modifications of the photooxidant properties of SRNOM induced by these
25 chemical changes. At 254 nm, UVC pre-irradiated SRNOM photodegraded glyphosate 29
26 times faster than original SRNOM and the reaction was fully inhibited by 2-propanol (5×10^{-3}
27 M). This enhanced photooxidant properties at 254 nm toward glyphosate was therefore
28 reasonably due to •OH radicals formation, as confirmed by additional ESR measurements. A
29 mechanism involving a chain reaction was proposed based on independent experiments
30 conducted on carbonyl compounds, particularly pyruvic acid and acetone. The findings of this
31 study show that UVC pre-treatment of NOM can enhance the removal of water pollutants and
32 suggests a possible integration of a NOM pre-activation step in engineered water treatment
33 systems.

34

35 Key-words: Natural organic matter, carbonyls, hydroperoxides, chain reaction, glyphosate,
36 •OH radicals

37

38

39

40 **Introduction**

41 Natural organic matter (NOM) is a complex mixture of organic compounds formed in
42 soils, sediments and natural waters as a result of microbial and chemical transformation of
43 plant tissues and microbial remains and it is an ubiquitous constituent of surface waters and
44 drinking water supplies. NOM needs to be removed in the process of drinking water
45 production because it can affect the color and organoleptic parameters of water and it can act
46 as a carrier of toxic organic compounds [Zoschke et al , 2012 ; Tang et al , 2014]. Under UVC
47 radiations (200-280 nm), typically used to remove bacterial and chemical contamination
48 [Sillanpää et al., 2018], NOM undergoes extensive degradation even though complete
49 mineralization is not usually achieved; the generation of potentially harmful by-products
50 originating from NOM degradation is a crucial aspect of drinking water production
51 [Buchanan et al, 2006]. Even though great efforts were put toward a better understanding of
52 the fate of NOM in UVC treatments [Ike et al, 2019 ; Paul et al, 2012 ; Varanasi et al, 2018 ;
53 Sarathy et al, 2011 ; Kulovaara et al, 1996; Schmitt-Kopplin et al, 1996 ; Corin et al, 1996 ;
54 Polewski et al, 2005 ; Lamsal et al, 2011; Rougé et al, 2020], many questions related to the
55 nature of intermediary photoproducts formed and their photoreactivity remain unanswered
56 and need to be further investigated.

57 Due to its heterogeneity and chemical complexity, NOM transformation was often
58 studied by monitoring global parameters using techniques such as absorption or fluorescence
59 spectroscopy, total organic carbon analysis, ¹³C NMR, pyrolysis and gel permeation
60 chromatography [Ike et al, 2019 ; Paul et al, 2012 ; Hao et al, 2020 ; Sarathy and Mohseni,
61 2007 ; Fukushima et al, 2001 ; Schmitt-Kopplin et al, 1996 ; Polewski et al, 2005]. These
62 analytical techniques allowed to assess an overall decrease of NOM UV-visible absorbance,
63 of aromaticity and of molecular weight during oxidation processes. Several studies focused on
64 the identification of small molecules, generated from NOM breakdown, by coupling

65 derivatization techniques with liquid chromatography-mass spectrometry (LC-MS) or gas
66 chromatography-mass spectrometry (GC-MS). Formation of C₁-C₄ carbonyl compounds and
67 C₂-C₅ carboxylic acids, amino acids and alcohols in UVC treatments was reported [Thomson
68 et al, 2004 ; Agbaba et al, 2016 ; Zhong et al, 2017 ; Corin et al, 1996]. Some of these
69 photoproducts were also found upon irradiation of NOM with natural or simulated solar-light
70 ($\lambda > 290$ nm) [Brinkmann et al, 2003 ; de Bryun et al, 2011 ; Goldstone et al, 2002 ; Kieber et
71 al, 1990].

72 The presence of NOM in UVC treatments has been generally reported to lower
73 treatment efficiency due to its ability to scavenge the reactive species generated under
74 irradiation and/or to absorb photons competitively, therefore decreasing the degradation rate
75 of target compounds [Wang et al, 2016]. However, NOM is able to generate oxidant species
76 such as hydroxyl radicals ($\bullet\text{OH}$), singlet oxygen ($^1\text{O}_2$) and triplet excited states ($^3\text{NOM}^*$)
77 under irradiation [Vione et al, 2014] and can also promote the degradation of contaminants
78 during UVC treatment [Lester et al, 2013]. The photosensitizing properties of NOM may
79 evolve during the UVC treatment because NOM itself undergoes chemical changes. Yet, to
80 the best of our knowledge, very few studies investigated the effect of such modifications on
81 the ability of NOM to generate photooxidants in the course of engineered water treatments.
82 Treatments of NOM with hypochlorous acid and ozone were reported to increase its capacity
83 to generate $^1\text{O}_2$ in simulated solar light due to the possible formation of quinone-like
84 molecules [Mostafa and Rosario-Ortiz, 2013 ; Leresche et al, 2019] but also to decrease its
85 capacity to generate $^3\text{NOM}^*$ due to photosensitizers destruction [Wenk et al, 2015]. On the
86 other hand, UV/chlorine treatment of NOM at high chlorine dosage was found to increase its
87 ability to generate $^3\text{NOM}^*$, $^1\text{O}_2$, and $\bullet\text{OH}$, upon irradiation within the range 290-400 nm
88 [Zhou et al, 2021]. Again, these effects were proposed to be due to the formation of quinone
89 and ketone functional groups.

90 The goal of this work was to study the chemical changes of SRNOM under UVC
91 irradiation and to determine how these changes affect its photodegrading properties. In the
92 first part, spectral changes of irradiated SRNOM solutions were monitored by UV-visible and
93 fluorescence spectroscopies while photoproducts were analyzed by derivatization of SRNOM
94 followed by liquid chromatography coupled to high resolution mass spectrometry (UHPLC-
95 HRMS) or gas chromatography coupled to mass spectrometry (GC-MS). In the second part,
96 we studied the effect of the UVC pre-irradiation on the photosensitizing properties of
97 SRNOM. For the experiments at 254 nm, we chose glyphosate, as a probe molecule, for two
98 reasons. It is non-absorbant at 254 nm and thus poorly subject to photolysis. Moreover, its
99 aliphatic and saturated structure makes it difficult to oxidize except by very oxidant species
100 such as •OH. The photooxidant properties of carbonyls at 254 nm was also studied for
101 comparison. For the experiments at $\lambda > 300$ nm, we used recommended probe molecules to
102 compare the formation of •OH, ³SRNOM* and singlet oxygen before and after UVC pre-
103 irradiation [Rosario-Ortiz and Canonica, 2016].

104

105 **Material and methods**

106 **Chemicals**

107 SRNOM (2R101N) was purchased from the International Humic Substances Society (IHSS).
108 Glyphosate (99.7%) and H₂O₂ (> 30%) were obtained from Fluka. Methylglyoxal (40% in
109 weight), pyruvic acid (98%), glycolic acid (98%), acetone (> 99.5%), 2,4,6-trimethylphenol
110 (TMP, certified reference material), furfuryl alcohol (FFA, analytical grade), terephthalic acid
111 (98%), hydroxyl-terephthalic acid (97%), 2,4-dinitrophenylhydrazine (DNPH, 97%),
112 bis(trimethylsilyl)trifluoro-acetamide containing 1% trimethylchlorosilane (BSTFA + 1%
113 TMCS, 98.5% excluding TMCS), NaH₂PO₄ (≥ 99.5%), Na₂HPO₄ (≥ 99%), horseradish
114 peroxidase (52 units per mg of solid), 4-hydroxyphenylacetic acid (98%), 5,5-dimethyl-1-

115 pyrroline-N-oxide (DMPO, > 98%) and catalase (2000-5000 units per mg of protein were
116 purchased from and Sigma Aldrich. Water was purified by reverse osmosis RIOS 5 and
117 Synergy, Millipore device, with resistivity 18 MΩ cm and DOC < 0.1 mg L⁻¹. All these
118 chemicals were used as received.

119 **UVC pre-irradiation of SRNOM**

120 Briefly, 10 mg of SRNOM were dissolved in 250 ml of purified water to reach a
121 concentration of 40 mg L⁻¹. SRNOM solutions were buffered at pH 7 using phosphate buffers
122 (10⁻³ M) except for experiments conducted to monitor the pH evolution during irradiation or
123 designed to the detection of carboxylic and hydroxylic intermediates. In these cases, SRNOM
124 solutions were neutralized to pH = 7 ± 0.2 using freshly prepared NaOH (0.1 M). All the
125 solutions were stored at 4°C. SRNOM solutions (30 mL) were poured in a quartz glass
126 cylindrical vessel (2 cm i.d. × 19 cm) and were irradiated in a device equipped with 4
127 germicidal tubes (253.7 nm, General Electric, 15 W). The photon flux entering the solution,
128 corresponding to 2.9 × 10⁻⁶ Einstein.L⁻¹.s⁻¹, was calculated by measuring the rate of
129 glyphosate loss in the presence of H₂O₂ (SI-Text 1, Fig SI-1). SRNOM solutions were
130 irradiated for 1 h, 2 h, 3 h and 4 h in separate experiments and labelled SRNOM_{1h}, SRNOM_{2h},
131 SRNOM_{3h}, and SRNOM_{4h}, respectively. Irradiated solutions were used for analyses or
132 sensitizing investigations within the 24 h following irradiation.

133

134 **Analysis of original and UVC pre-irradiated SRNOM**

135 UV-visible spectra were recorded on a Varian Cary 3 UV-Vis spectrophotometer.
136 Fluorescence spectra were recorded using a Perkin Elmer LS 55 Luminescence Spectrometer.
137 The excitation wavelength was set at 255 nm and the absorbance of solutions was adjusted at
138 0.10 ± 0.01 at 255 nm by dilution with purified water. The emission spectra were corrected
139 for the dilution coefficient. Dissolved organic carbon (DOC) was measured using a Shimadzu

140 5050 TOC analyser. Carbonyls contained in SRNOM and irradiated SRNOM were analyzed
141 by DNPH derivatization [Soman et al, 2008] (SI Text 2). Analyses were performed by ultra-
142 high performance liquid chromatography (UHPLC) coupled to high resolution mass
143 spectrometry (HRMS). HRMS was performed on an Orbitrap Q-Exactive (ThermoScientific)
144 coupled to Ultimate 3000 RSLC (ThermoScientific) UHPLC. Analyses were run in negative
145 (ESI) electrospray modes. The column was a Kinetec EVO C₁₈ 100 mm / 2.1 mm, 1.7 μm
146 (Phenomenex). Details of separation conditions are given in (SI Text 3). Molecular formulas
147 were obtained setting the difference between experimental and accurate masses to ≤ 5 ppm
148 while structures are proposed based on the number of DNPH molecules linked to carbonyls
149 and on the number of double bonds in the carbonyl (NDB). In several cases, several isomers
150 are possible and given structures are thus only indicative. Pyruvic acid and methylglyoxal
151 were used as references to estimate the concentration of the other carbonyls (SI Text 3 and
152 Fig. SI-2).

153 Carboxylic and hydroxylic intermediates were detected by a method using BSTFA
154 derivatization (SI Text 4) followed by analysis with gas chromatography/electron impact MS
155 (GC/EI-MS) [Yu et al, 1998]. Solutions were analyzed on an Agilent 6890N Network gas
156 chromatograph coupled to a 5973 Network mass selective detector and Agilent 7683B series
157 injector. Data acquisition and processing and instrument control were performed by Agilent
158 MSD ChemStation software. Separation conditions are described in (SI Text 4). Mass spectra
159 were scanned between m/z 50 and m/z 500 with the source temperature set at 230°C.
160 Identification was based on matching query spectra to spectra present in the reference library
161 (NIST17), with a minimum spectral similarity measure of 95%. Glycolic acid was derivatized
162 by BSTFA as for SRNOM samples and used as a reference for the quantification of other
163 compounds.

164 SRNOM and SRNOM_{3h} were also analyzed by ionic Chromatography-Mass spectrometry (IC-
165 MS). Details are given in SI-text 5.

166

167 **Sensitizing properties of original and UVC pre-irradiated SRNOM**

168 Glyphosate was used to probe the formation of very oxidant species such as •OH from
169 original and pre-irradiated SRNOM solutions at 254 nm. The solutions containing glyphosate
170 (10^{-5} M) and SRNOM were prepared by adding 25 μ L of the stock solution of glyphosate (10^{-2}
171 M) to 10.2 mL of SRNOM (40 mg L^{-1}) and by adding purified water to reach the final
172 volume of 25 mL. For SRNOM_{3h} solutions, the same spike of glyphosate was added to 25 mL
173 of non diluted solution. This way, the two solutions showed the same absorbance of 0.34 at
174 254 nm. Then, 15 mL of each solution were irradiated in the above-described device. 2-
175 Propanol was used as a quencher of •OH. Glyphosate (10^{-5} M) was also irradiated in the
176 presence of acetone (10^{-4} M), pyruvic acid (10^{-4} M), H₂O₂ (10^{-5} M), acetone (10^{-4} M) + H₂O₂
177 (10^{-5} M). Furthermore, acetone (10^{-4} M) was irradiated alone and in mixture with H₂O₂ (10^{-5}
178 and 10^{-3} M). All these experiments were conducted in air-saturated solutions. The effect of
179 oxygen on the rate of glyphosate photodegradation in the presence of SRNOM_{3h} was studied
180 by saturating the solution with N₂. Glyphosate concentration was monitored by UHPLC-
181 HRMS by integrating peak area at $m/z = 168.0056 (\pm 5 \text{ ppm})$. AMPA
182 (aminomethylphosphonic acid) with $m/z = 110.0002 (\pm 5 \text{ ppm})$ was the only glyphosate
183 photoproduct detected. Acetone loss and photoproducts formation were monitored by
184 derivatization with DNPH followed by UHPLC-HRMS analysis. Photodegrading properties
185 of SRNOM and SRNOM_{3h} solutions were also investigated under irradiation between 300 and
186 400 nm. Both solutions were diluted by a half during preparation of mixtures. Terephthalic
187 acid (2×10^{-5} M) was used to probe •OH radicals, 2,4,6-trimethylphenol (2×10^{-5} M) to probe
188 ³SRNOM* and ³SRNOM_{3h}* and furfuryl alcohol (5.8×10^{-5} M) to trap ¹O₂. Solutions

189 buffered at pH 7 were irradiated in a device equipped with 6 fluorescent tubes emitting
190 between 300 and 400 nm [Palma et al, 2020]. Pseudo-first-order rate constants of probes
191 phototransformation were determined by plotting $\ln(C_t/C_0) = k \times t$, where C_t and C_0 are the
192 probe concentration at time t and before irradiation. All the experiments were duplicated.

193

194 **Peroxides titration**

195 Peroxides concentration was measured by the spectrofluorimetric quantification method
196 previously described by Miller and Kester, 1988. Details of the experiments are given in SI-
197 text 6.

198

199 **ESR experiments**

200 ESR experiments were carried out using a Bruker EMX, 9.8 GHz equipped with a cavity
201 ER4105DR and a xenon lamp (Xenovia 200 - 900 nm). The ESR spectra were obtained at
202 room temperature under irradiation inside the cell of the following mixtures : DMPO (25
203 mM) in the presence of SRNOM (20 mg L^{-1}), SRNOM_{3h} or H₂O₂ (5×10^{-3} or 10^{-5} M).

204

205 **Results and discussion**

206 **1. Spectral changes of SRNOM upon 254-nm irradiation**

207 Fig. 1A shows that the SRNOM solution progressively photobleached. The absorbance
208 at 254 nm declined by 59% and 77% after 3 and 4 h of irradiation, respectively (Table 1). The
209 reduction of DOC as a function of irradiation time revealed that SRNOM also underwent
210 substantial mineralization (35% after 4 h) while the specific ultraviolet absorbance (SUVA)
211 decreased by 42% and 64% after 3 and 4 h of irradiation, respectively, indicating a loss of
212 unsaturated/aromatic moieties [Weisshar et al, 2003] (Table1). Yet, the spectrum shape (Fig.

213 1B) and the E_2 / E_3 ratio (Table 1) did not change much indicating that photoproducts
214 negligibly contributed to the absorption and were poorly absorbing compounds.

215 Irradiation also led to a breakdown of fluorescent species in accordance with previous
216 studies [Patel-Sorrentino et al, 2004]. The fluorescence intensity at the emission maximum
217 declined by 53% after 3 h of irradiation, and by 68% after 4 h (Fig 1 C). Fig 1D also shows
218 that the blue part of the fluorescence emission spectra disappeared the fastest leading to
219 emission spectra red-shifted by 10 - 15 nm or to a band contraction. On the contrary,
220 treatment of NOM with radicals such as $\text{SO}_4^{\bullet-}$ [Zhang et al, 2019] or $\bullet\text{OH}$ [Varanasi et al,
221 2018] was reported to induce a blue-shift of fluorescence emission spectra attributed to
222 preferential degradation of high molecular weight moieties into smaller entities. In these
223 treatments, radicals are expected to react preferentially with biggest macromolecules offering
224 the largest number of attack sites while in photolytic treatment the reactivity of generated
225 excited states is the critical factor. Our results suggest that smaller fluorescent entities initially
226 present in SRNOM or produced in the course of the treatment were more subject to
227 photodegradation than larger ones. The reasons could be that they were more light absorbing
228 because more oxidized and/or underwent less desactivation processes than bigger constituents
229 being less embedded in large structures than these latter.

230

231 **2. Carbonyls and carboxylic acids formation upon 254-nm irradiation of SRNOM**

232 Table 2 summarizes the chemicals detected by DNPH or BSTFA derivatization and by
233 CI/MS in SRNOM before irradiation and after irradiation. Detailed MS data are given in
234 Figure SI-3, Tables SI-1 to SI-3 and the structures of photoproducts observed in irradiated
235 samples are shown in Figure 2. In starting SRNOM, we detected 5 carbohydrates in C_5 and C_6
236 (xylose, rhamnose, fucose, glucose and galactose) mentioned in the IHSS web page, along
237 with 2 monocarboxylated alkanes in C_3 and C_{18} (glyceric and oleic acids) and 3

238 dicarboxylated alkanes in C₆, C₉ and C₁₂ (hexanedioic, nonanedioic and dodecanedioic acids)
239 (Tables 2 and SI-1). Several carbonyls were found, but only as traces.

240 In SRNOM_{3h}, none of the carbohydrates observed in SRNOM were found while 11
241 carboxylated alkanes were detected: 5 monocarboxylated in C₁ (formic acid), C₂ (acetic and
242 glycolic acid), C₃ (lactic acid) and C₄ (4-aminobutanoic acid), 7 dicarboxylated alkanes in C₂
243 (oxalic acid), C₃ (malonic, tartronic, dihydroxymalonic acids), C₄ (butanedioic and malic
244 acids), C₅ (glutaric acid) and C₆ (tricarballic acid) (Tables 3 and SI-2). In all the irradiated
245 samples, 16 carbonyls in C₁-C₅ were detected among them 7 monocarbonyls (formaldehyde,
246 acetaldehyde, glycolaldehyde, glyoxylic acid), 7 dicarbonyls (glyoxal, methylglyoxal,
247 butenedial) and 2 tricarbonyls. Some of these compounds were already reported to be
248 produced by irradiation of natural surface waters or synthetic waters containing NOM with
249 natural or simulated solar-light, by ozone treatment or by UV-based AOPs of solutions of
250 humic substances. This is the case for formic, acetic and oxalic acids [Brinkmann et al, 2003 ;
251 Goldstone et al , 2002], formaldehyde, acetaldehyde, glyoxal and methylglyoxal [Thomson et
252 al, 2004 ; Agbaba et al, 2016 ; Zhong et al, 2017 ; de Bryun et al, 2011 ; Kieber et al, 1990],
253 malonic and butanedioic acids [Corin et al, 1996], and pyruvic acid [Thomson et al, 2004].

254 The concentration of the different carbonyls after 1, 2, 3 and 4 h of irradiation were
255 estimated using derivatized methylglyoxal and pyruvic acid (Table SI-4). Figure 3A shows
256 the concentration profile of the most concentrated ones, i.e. formaldehyde, glyoxylic acid,
257 pyruvic acid, glyoxal and glycolaldehyde, as a function of irradiation time. The concentration
258 of formaldehyde and glyoxylic acid was maximum after 2 h of irradiation and then declined
259 while that of pyruvic acid, glyoxal and glycolaldehyde increased throughout the 4 h of
260 irradiation. It shows that SRNOM photodegradation still proceeds beyond 4 h although a
261 significant absorbance decrease at 254 nm.

262 The total pool of C₁-C₅ carbonyls was estimated by summing the individual
263 concentrations. Figure 3B shows that their cumulative concentration increased during the first
264 2 h of irradiation to reach the value of 2.8×10^{-4} M. Based on these concentrations and on the
265 DOC measurements, the mass percentage of carbon atoms contained in the detected carbonyls
266 could be calculated using Eq 1. This percentage was maximum after 3 h of irradiation where it
267 reached 46% (Figure 3B). This high value demonstrates the very important contribution of
268 C₁-C₅ carbonyls to the pool of photoproducts. As most of these compounds poorly absorbed
269 below 300 nm, their high concentration explains the unchanged spectrum shape following
270 irradiation.

271

$$272 \quad \text{Mass percentage}_t = \frac{\sum_{i=1}^{i=n} [c_i]_t \times M_i}{\text{DOC}_t} \quad \text{Eq 1}$$

273 where $[c_i]_t$ and M_i are the concentration at time t and the molecular mass of carbonyl i, and
274 DOC_t is the organic carbon content in the solution at time t.

275 The concentration of carboxylic acids detected in SRNOM_{3h} are shown in Table SI-5.
276 In general, BSTFA-GC-MS and CI-MS analyses gave consistent results regarding the
277 concentration estimations. BSTFA-GC-MS was however less performant than CI-MS in the
278 analysis of compounds containing 2 or 3 CO₂H or OH functions such as tartronic,
279 dihydroxymalonic acid, oxalic acid and tricarballylic acids. The difficulty to solubilize
280 lyophilized SRNOM_{3h} in acetonitrile to conduct the BSTFA derivatization or a partial
281 derivatization of these compounds probably explain these discrepancies. Malic, oxalic,
282 butanedioic, glycolic, and malonic acids were the most concentrated acids. However, their
283 concentration in SRNOM_{3h} that laid below 2.8×10^{-6} M, were much lower than those of
284 carbonyls. Eq 1 allowed to determine that the detected carboxylic acids contained only 2% in
285 mass of the SRNOM_{3H} carbon atoms.

286 Nitrate ions were also detected by CI-MS in SRNOM at a level of 2.9×10^{-6} M, but
287 not in SRNOM_{3h}.

288 The detection of all these compounds suggests that the photodegradation of SRNOM
289 under UVC resulted from a complex set of reactions involving the direct photolysis of
290 SRNOM constituents as well as their oxidation by the radicals generated in the course of the
291 irradiation. Many radicals such as R•, RO•, RO₂•, HO₂•/O₂• and •OH can be formed by C-C,
292 C-O, and O-O bond cleavage, phenyl-O⁻ and RCO₂⁻ photoionization, addition of oxygen on
293 radicals and various radical attacks. Once formed, these radicals could contribute to further
294 degradation of SRNOM constituents and of their by-products. Among them, •OH radical is
295 likely to play a significant role for several reasons. It is the most oxidant species able to react
296 with a wide variety of chemicals by addition on double bonds or by H atom abstraction
297 [Buxton et al, 1988]. NOM was shown to generate •OH radicals [Vaughan and Blough, 1998 ;
298 Page et al, 2011; McKay et al, 2015 ; Gan et al, 2008 ; Sun et al, 2015 ; Dong et al, 2012 ;
299 Aguer and Richard, 1999] under irradiation. In reactions where •OH radicals are purposely
300 produced [Varanasi et al, 2018] the oxidation degree of photoproducts, given by the O/C ratio,
301 is generally high (1-2), as observed here. Last, the photolysis of chlorosalicylic acid, that was
302 proposed to occur via the intermediary formation of •OH radicals [Tafer et al, 2016], yielded
303 glycolic, lactic, and butanedioic acids, acetaldehyde, glycoaldehyde, methylglyoxal, C₄H₄O₃,
304 and C₃O₃H₂ that were also detected in the present work.

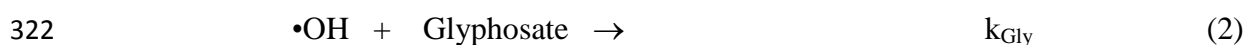
305

306 **3. Effect of SRNOM pre-irradiation on the oxidant properties at 254 nm**

307 In order to explore the photooxidant properties of pre-irradiated SRNOM, we chose
308 glyphosate as a chemical probe. We first checked that it is photostable when irradiated in our
309 device ($k < 2 \times 10^{-4} \text{ min}^{-1}$, Table 3). For these experiments, we selected SRNOM_{3h} that
310 showed the highest concentration of intermediary carbonyl compounds (2.4×10^{-4} M) and

311 SRNOM and SRNOM_{3h} were tested at the same absorbance at 254 nm (0.34). In the presence
 312 of SRNOM, glyphosate (10⁻⁵ M) disappeared with a rate constant k of 0.0013 ± 0.0002 min⁻¹
 313 in air-saturated solution (Figure 4A and Table 3). Making the hypothesis that the reaction was
 314 due to the reaction of glyphosate with •OH radicals, we used this rate constant to estimate the
 315 quantum yield of •OH radicals formation by SRNOM (Φ_{OH}^{SRNOM}) in the first stages of the
 316 reaction. Once formed by process 1, •OH radicals react with glyphosate ($k_{gly} = (3.37 \pm 0.10) \times$
 317 $10^7 \text{ M}^{-1} \text{ s}^{-1}$, Vidal et al, 2015) (process 2) and with SRNOM (process 3). We took for k_{SRNOM}
 318 the value of $1.6 \times 10^8 \text{ M}_C^{-1} \text{ s}^{-1}$ reported in the literature for Suwannee river fulvic acid
 319 [Westoffer et al, 2007].

320



324

325 The rate of glyphosate photodegradation (R_{Gly}) can be written (SI-Text 7):

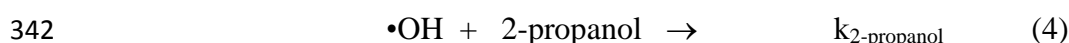
326

$$R_{Gly} = I_0 (1 - 10^{-A_{SRNOM}}) \Phi_{OH}^{SRNOM} \frac{k_{gly} [Gly]}{k_{gly} [Gly] + k_{SRNOM} [SRNOM]} \quad EQ1$$

327

328 where $I_0 (1 - 10^{-A_{SRNOM}})$ is the rate of light absorption by SRNOM. As SRNOM was diluted
 329 2.44 fold to reach the same absorbance at 254 nm as SRNOM_{3h}, [SRNOM] was equal to 6.35
 330 mgC L⁻¹ or 0.529 mM_C⁻¹, taking 12 for the molar mass of carbon. In these conditions, one
 331 gets that glyphosate trapped 0.38% of •OH radicals and that Φ_{OH}^{SRNOM} was equal to 0.024;
 332 this value is in the range of that reported by Lester et al (2013) at 254 nm (0.047).

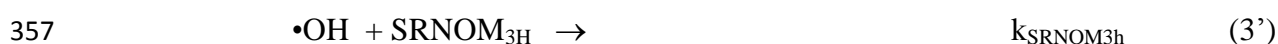
333 In the presence of SRNOM_{3h} and in air-saturated solution, glyphosate disappeared
 334 much faster than in the presence of SRNOM (Figure 4A) with $k = 0.038 \pm 0.004 \text{ min}^{-1}$ (Table
 335 3). In N₂-purged SRNOM_{3h} solution, the glyphosate photodegradation rate was significantly
 336 reduced compared to the one conducted in air-saturated medium ($k = 0.002 \pm 0.002 \text{ min}^{-1}$ in
 337 the first 10 min of the reaction, Figure 4A, Table 3) demonstrating the important role played
 338 by oxygen in the reaction. Moreover, we irradiated glyphosate and SRNOM_{3h} in the presence
 339 of 2-propanol to determine whether •OH radicals were involved in the loss of glyphosate.
 340 Using $k_{2\text{-propanol}} = 1.9 \times 10^9 \text{ M}^{-1} \text{ s}^{-1}$ [Buxton et al, 1998] for the bimolecular rate constant of
 341 reaction between •OH and 2-propanol :



343 we added $5 \times 10^{-3} \text{ M}$ of 2-propanol expecting an inhibition of the reaction > 90% based on
 344 $k_{\text{SRNOM}_{3h}}[\text{SRNOM}_{3h}] \sim 9 \times 10^4 \text{ s}^{-1}$, as for SRNOM. The inhibition was of 90% (Figure 4A,
 345 Table 3) in accordance with a significant contribution of •OH.

346 Spin trap experiments using DMPO as the spin-trapping reagent were also conducted
 347 to confirm the formation of •OH radicals. Figure 5 shows that the four-line signal with an
 348 intensity ratio 1:2:2:1 characteristic of the DMPO-OH• adduct was not detected when DMPO
 349 was irradiated in the presence of SRNOM (plot a) or H₂O₂ (10^{-5}) (plot c) while it was
 350 observed with SRNOM_{3h} (plot b) and H₂O₂ ($5 \times 10^{-3} \text{ M}$) (plot d). Again, this result is in line
 351 with the production of •OH radicals upon irradiation of SRNOM_{3h} in UVC.

352 Postulating that the disappearance of glyphosate was only due to the reaction with
 353 •OH, we made the same calculation for SRNOM_{3h} as for SRNOM, after having replaced
 354 processes 1 and 2 by processes 1' and 3' respectively:



358

359 and substituting SRNOM by SRNOM_{3h} in EQ1. The TOC analyses showed that SRNOM_{3h}
360 had a DOC content of 10.9 mgC L⁻¹ or 0.907 mM_C⁻¹ (Table 1). To estimate the percentage of
361 •OH radicals reacting with glyphosate in SRNOM_{3h} solution, we also need to know the value
362 of k_{SRNOM3h}. Since SRNOM_{3h} is much less aromatic than SRNOM, and •OH radicals react
363 more easily with aromatic or conjugated structures than with saturated ones, k_{SRNOM3h} is
364 possibly smaller than k_{SRNOM}. Postulating that the rate constant decrease may parallel the
365 absorbance decrease at 254 nm, we opted for k_{SRNOM3h} = (0.7 ± 0.3) × 10⁸ M_C⁻¹ s⁻¹. From this
366 value, the percentage of •OH radicals trapped by glyphosate in SRNOM_{3h} solution would lay
367 between 0.3 and 0.8 % and Φ_{OH}^{SRNOM3h} would be comprised between 0.21 and 0.55, a value
368 between 10 and 20 times higher than that found for Φ_{OH}^{SRNOM}. This value must be considered
369 as a maximal value and would be lower if radicals other than •OH also contributed to the
370 degradation of glyphosate. To better understand the enhancing effect of the pre-irradiation on
371 the photooxidant properties of SRNOM, we conducted additional experiments and tested
372 potential candidates for their ability to photodegrade glyphosate.

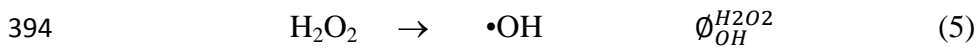
373

374 **4. Peroxides formation and role of H₂O₂ in the oxidant properties at 254 nm**

375 Peroxides are sources of •OH radicals through direct photolysis (process 5) or photo-
376 Fenton reaction and we quantified their formation in our system. Measurements of H₂O₂ and
377 RO₂H + RO₂R were performed on SRNOM and SRNOM_{3h} irradiated for 30 min (Figure 5).
378 In SRNOM, H₂O₂ and RO₂H + RO₂R accumulated linearly. After 30 min of irradiation, the
379 total concentration of H₂O₂ + RO₂H + RO₂R was equal to 16 μM; H₂O₂ was by far the most
380 abundant species (14.2 μM) while RO₂H + RO₂R contributed to the pool of peroxides in a
381 minor way (1.8 μM). In SRNOM_{3h}, the peroxides formation was auto-inhibited, slowing
382 down after 10 min. The total concentration reached 15.8 μM after 30 min ; H₂O₂ and RO₂H +

383 RO₂R were in equivalent amounts of ~ 8.0 μM. The formation of H₂O₂ in the photolysis of
 384 NOM is well documented in the literature [Garg et al., 2011]. It is formed by dimutation of
 385 O₂⁻ that arises from reduction of dissolved O₂. Peroxides and hydroperoxides are generated
 386 after the reaction of R[•] radicals with dissolved O₂ to yield RO₂[•] and the reaction of these
 387 peroxy radicals with O₂⁻/HO₂[•] [Sun et al., 2021].

388 To determine the contribution of H₂O₂ to the formation of •OH via process (5), we
 389 proceeded as follows. We first measured R_{Gly} in the presence of H₂O₂ (10⁻⁵ M) alone. The
 390 value of 1.5 × 10⁻⁹ M⁻¹ s⁻¹ allowed us to check that glyphosate reacted with •OH and to
 391 measure the photon flux I₀ in the irradiation device (SI-Text 1). Then, we calculated R_{Gly}^{H2O2}
 392 in SRNOM solution using Eq 2, supposing that the photolysis of H₂O₂ produced during the
 393 irradiation of SRNOM was the only source of •OH through process 5 (SI-Text 5).



395

$$R_{\text{Gly}}^{\text{H}_2\text{O}_2} = I_{a,\text{H}_2\text{O}_2}^{\text{SRNOM}} \Phi_{\text{OH}}^{\text{H}_2\text{O}_2} \frac{k_{\text{gly}} [\text{Gly}]}{k_{\text{gly}} [\text{Gly}] + k_{\text{SRNOM}} [\text{SRNOM}] + k_{\text{H}_2\text{O}_2} [\text{H}_2\text{O}_2]} \quad \text{EQ2}$$

396

397 Taking [H₂O₂] = 14 μM (corresponding to the highest value reached for SRNOM), ε_{H2O2} =
 398 19.6 M⁻¹ cm⁻¹ at 254 nm, A₂₅₄ = 0.34 for SRNOM and ℓ = 2, we calculated I_{a,H2O2}^{SRNOM} using the
 399 Beer-Lamber law for a mixture (SI-Text 8). Then, taking k_{H2O2} = 2.7 × 10⁷ M⁻¹.s⁻¹ [Stephan et
 400 al, 1996], we got that glyphosate trapped 0.38% of •OH and using Φ_{OH}^{H2O2} = 1 [Yu and
 401 Barker, 2003], we finally obtained R_{Gly}^{H2O2} = 7.0 × 10⁻¹² M s⁻¹. In the case of SRNOM_{3h}, we
 402 took [H₂O₂] = 8 μM and the same calculation led to R_{Gly}^{H2O2} = (3.0-9.0) × 10⁻¹² M s⁻¹. Both
 403 values are very small compared to the experimental values 2.2 × 10⁻¹⁰ M s⁻¹ and 6.5 × 10⁻⁹ M
 404 s⁻¹ respectively measured for SRNOM and SRNOM_{3h} and it can be concluded that the
 405 photochemical decomposition of titrated hydroperoxides negligibly contributed to the

406 oxidation of glyphosate. Spontaneous decomposition of unstable hydroperoxides into RO•
407 and •OH might be an alternative source of •OH radicals. This was considered by Badiali et al
408 (2015) and Krapf et al (2016) in their studies on secondary organic aerosols.

409

410 **5. Role of carbonyls in the photooxidant properties at 254 nm**

411 Given the high concentration of carbonyls detected in SRNOM_{3h} and the known
412 potential of these chemicals as sensitizers, we tested if they could induce the transformation of
413 glyphosate at 254 nm. We first tested pyruvic acid since this compound had been previously
414 detected in our irradiated SRNOM samples. In the presence of this ketoacid (10⁻⁴ M), in pH 7
415 buffered solutions, glyphosate (10⁻⁵ M) disappeared with an apparent first order rate constant
416 equal to 0.021 ± 0.002 min⁻¹ (Figure 6A, Table 3). Pyruvate was also photodegraded and the
417 reaction auto-accelerated. During the first 6 min of irradiation, only 1.8 × 10⁻⁶ M of pyruvate
418 were transformed against 3.1 × 10⁻⁵ M between 6 and 30 min (Figure 6B). The rate of
419 pyruvate loss, R_{pyruvate}, in the second part of the curve was equal to 2.1 × 10⁻⁸ M s⁻¹, and R_{Gly}
420 to 3.5 × 10⁻⁹ M s⁻¹. The experiment was repeated in the presence of 2-propanol added to trap
421 •OH radicals. The concentration 10⁻⁴ M was chosen for 2-propanol for a theoretical trapping
422 of more than 95% based on k_{pyruvate acid} = 3 × 10⁸ M⁻¹ s⁻¹ (process 6) [Buxton et al, 1998]. After
423 30 min, the rate of glyphosate loss was reduced by 75% confirming a significant contribution
424 of •OH in the reaction.



426

427 Although it was not detected in irradiated SRNOM samples, acetone was chosen to
428 represent monocarbonyls because it is a simple molecule, it can be purchased in high purity, it
429 was already studied and its quantum yield of photolysis is known ($\Phi_{\text{acetone}} = 0.061$ at 270 nm,
430 Anpo and Kubokawa, 1977). At 10⁻⁴ M, a concentration falling within the range of that found

431 for intermediary carbonyls, acetone increased the rate of glyphosate photodegradation and the
 432 reaction was also auto-accelerated (Figure 6A, Table 3). During the first 10 min of reaction,
 433 an averaged $k = 0.002 \pm 0.001 \text{ min}^{-1}$ was obtained while, between 10 and 30 min, we
 434 measured $k = 0.024 \pm 0.003 \text{ min}^{-1}$. In parallel, the decay of acetone was monitored by
 435 UHPLC-HRMS after DNPH derivatization. Acetone also disappeared by an autoaccelerated
 436 reaction (Figure 6B). Between 0 and 10 min, the loss of acetone was lower than 5%
 437 corresponding to a rate of acetone photodegradation (R_{acetone}) $< 0.9 \times 10^{-8} \text{ M s}^{-1}$ while,
 438 between 10 and 40 min, acetone disappeared by 43% and R_{acetone} was equal to $2.4 \times 10^{-8} \text{ M s}^{-1}$
 439 (Table 3). During this reaction H_2O_2 was formed (Figure 6B). The H_2O_2 production was of 2
 440 μM between 0 and 10 min and 10 μM between 10 and 30 min which mirrored the
 441 autoaccelerated decrease of glyphosate and acetone. In the presence of 2-propanol (10^{-4} M)
 442 and acetone (10^{-4} M), glyphosate disappeared by 10% instead of 42% in the absence of 2-
 443 propanol after 30 min of irradiation (Figure 6A, Table 3) confirming again a significant
 444 contribution of $\bullet\text{OH}$ in the reaction (75%).

445 Acetone was also irradiated alone to check that the observed auto-acceleration was not
 446 due to the presence of glyphosate. At $2.4 \times 10^{-4} \text{ M}$, acetone also disappeared in an auto-
 447 accelerated reaction with $R_{\text{acetone}} < 0.9 \times 10^{-8} \text{ M}^{-1} \text{ s}^{-1}$ between 0-10 min and $R_{\text{acetone}} = 3.9 \times 10^{-8}$
 448 $\text{M}^{-1} \text{ s}^{-1}$ between 10-30 min (Table 3). The photoproducts were pyruvic acid, methyl glyoxal,
 449 hydroxyacetone, formadehyde as described by Stephan and Bolton (1999) when they studied
 450 the photolysis of acetone in the presence of H_2O_2 at 254 nm. Using the quantum yield of
 451 acetone photodegradation in diluted solutions (0.061), and $\epsilon_{\text{acetone}} = 16 \text{ M}^{-1} \text{ cm}^{-1}$ at 254 nm, it
 452 is possible to calculate the rate of acetone photodegradation by direct photolysis
 453 R_{acetone}^{dp} using EQ3:

454

$$R_{\text{acetone}}^{dp} = I_0 \left(1 - 10^{-A_{\text{acetone}}}\right) \phi_{\text{acetone}} \quad \text{EQ3}$$

455

456 For [acetone]= 10^{-4} M, one gets $R_{acetone}^{dp} = 1.3 \times 10^{-9}$ M s⁻¹ and for [acetone]= 2.4×10^{-4} M
457 $R_{acetone}^{dp} = 3.1 \times 10^{-9}$ s⁻¹. These values are consistent with the ones obtained between 0 and
458 10 min ($< 9 \times 10^{-9}$ M s⁻¹), and one can conclude that $R_{acetone}^{dp}$ being negligible behind $R_{acetone}$
459 measured in the second part of the curves, other reactions should take place.

460 An autoaccelerated reaction is generally due to the accumulation of key intermediates.
461 Here, the intermediary chemicals were the acetone photoproducts and peroxides, among
462 which, H₂O₂. We therefore studied the effect of H₂O₂, used a hydroperoxide model, at the
463 concentration of 10^{-5} and 10^{-3} M on the photodegradation of acetone (2.4×10^{-4} M). The
464 photodegradation of acetone was fast till the very beginning of the irradiation ($R_{acetone} = 3.5 \times$
465 10^{-8} and 1.8×10^{-7} M s⁻¹, respectively, Table 3) and no auto-accelerating effect was observed.
466 In this mixture, acetone can disappear by reaction with •OH produced from H₂O₂ photolysis
467 (process 7, $k_{acetone} = 1.1 \times 10^8$ M⁻¹ s⁻¹, Buxton et al, 1998). Process 8 is a potential competing
468 pathway of •OH disappearance ($k_{H_2O_2} = 2.7 \times 10^7$ M⁻¹ s⁻¹ Buxton et al, 1998).

469



472

473 For [H₂O₂] = 10^{-3} M and [acetone] = 2.4×10^{-4} M, process 8 was expected to significantly
474 reduce the percentage of •OH radicals trapped by acetone. Taking into account that acetone
475 should trap about 50% of •OH, one obtains $R_{acetone} = 1.3 \times 10^{-7}$ M.s⁻¹ against 1.8×10^{-7} M s⁻¹
476 measured experimentally. For [H₂O₂] = 10^{-5} M and [acetone] = 2.4×10^{-4} M, process 8 was
477 negligible, and acetone was expected to trap all the •OH radicals produced by H₂O₂
478 photolysis. Its rate of decay through process 7 ($R_{acetone}^{OH}$) was equal to 2.6×10^{-9} M s⁻¹
479 according to EQ 4.:

$$R_{acetone}^{OH} = I_0 \left(1 - 10^{-A_{H_2O_2}} \right) \phi_{OH}^{H_2O_2} \quad EQ4$$

480

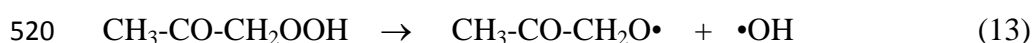
481 This calculated rate accounted for only 6.6% of the measured rate indicating that an additional
 482 radical source was responsible for acetone degradation. Then, we simultaneously irradiated
 483 glyphosate (10^{-5} M), H_2O_2 (10^{-5} M) and acetone (10^{-4} M). In this case, the glyphosate
 484 photodegradation was fast till the beginning of the irradiation ($k = 0.016 \text{ min}^{-1}$) (Figure 6A,
 485 Table 3) showing that H_2O_2 or other hydroperoxides are important intermediaries in the
 486 reaction.

487 The results obtained for acetone can be tentatively explained by the chain-reaction
 488 mechanism shown in Scheme 1. In the classical chain oxidation of a chemical RH bearing a
 489 labile H atom, the initiator produces the primary radicals (process 9) that start the chain
 490 through a transfer reaction by generating the radical $R\cdot$ (process 7). Then $R\cdot$ produces $RO_2\cdot$
 491 by adding O_2 (process 10) and $RO_2\cdot$ regenerates $R\cdot$ along to RO_2H by abstracting of a H from
 492 RH (process 11). The longer the chain length, the faster the reaction; in fact, when the chain is
 493 long enough, the rate of the propagation reactions becomes much higher than the rates of
 494 initiation and of transfer. In our case, the calculated rate of acetone photolysis $R_{acetone}^{dp}$
 495 (process 9) was much lower than the experimental rate of acetone photodegradation
 496 consistently with the involvement of a chain reaction.

497 The irradiation of acetone was expected to yield radicals by α -cleavage of the triplet
 498 excited state (process 9) [Pearson, 1963]. The triplet could also abstract a H-atom from
 499 methyl groups of acetone, however, neither acetone itself nor glyphosate were concentrated
 500 enough to compete significantly with the cleavage [Anpo and Kubokawa, 1977]. Due to the
 501 oxidation of these radicals and to the photolysis of the formed hydroperoxides, there should
 502 be a pool of initiating radicals in the system. The acetyl radical, $R\cdot$, formed by process 7
 503 [Stephan et al, 1996] should easily react with oxygen (process 10) to yield the peroxy radical

504 ROO• [Stephan et al, 1996]. This peroxy radical likely abstracted an H-atom from acetone
505 (process 11) to regenerate the acetyl radical and produce the hydroperoxide ROOH. The
506 recombination of two peroxide radicals (process 12) terminated this chain reaction.

507 In this chain reaction, glyphosate might be oxidized by several of the radicals
508 formed in the complex mixture. However, while the reaction with •OH was evidenced, the
509 oxidation with the other radicals remains to be demonstrated. If we make the hypothesis that
510 •OH contributed significantly to the glyphosate degradation, the source of •OH needs to be
511 explained. Indeed, calculations showed that the photolysis of the different hydroperoxides did
512 not yield enough radicals to explain the high rate of glyphosate degradation. An alternative
513 formation of •OH could be the spontaneous decomposition at room temperature of unstable
514 hydroperoxides, here CH₃-CO-CH₂OOH (process 13). According to the works of Badiali et al
515 (2015) and Krapf et al (2016), the formation of very unstable hydroperoxides is plausible.
516 Therefore, despite processes 7, 10 and 11 still taking place, the key process became process
517 13 since it introduced a continuous source of •OH and RO• radicals. Consequently, the rate of
518 glyphosate degradation increased during the accumulation phase of ROOH, reaching the
519 maximal value rate when the RO₂H formation equaled the RO₂H decomposition.



521 In the case of SRNOM_{3h}, carbonyls were present at 2.4×10^{-4} M and hydroperoxides
522 were potentially generated at a fast rate, therefore making it possible the mechanism already
523 proposed in the case of acetone to occur. In accordance, ROOH + ROOR were formed along
524 with H₂O₂. In SRNOM_{3h} solution, R_{gly} was equal to 6.3×10^{-9} M s⁻¹. Considering that
525 glyphosate trapped between 0.3 and 0.8 % of •OH radicals in competition with SRNOM_{3H}
526 constituents, the rate of •OH formation should be comprised between $\sim 8 \times 10^{-7}$ and 2×10^{-6}
527 M s⁻¹. In the model solution containing glyphosate (10^{-5} M), H₂O₂ (10^{-5} M) and acetone (10^{-4}
528 M), R_{gly} was equal to 2.7×10^{-9} M s⁻¹. Considering that •OH contributed to the reaction at

529 75% and that glyphosate trapped 3% of •OH in competition with acetone, then the rate of •OH
530 formation should be equal to $\sim 7 \times 10^{-8} \text{ M s}^{-1}$. For acetone ($2.4 \times 10^{-4} \text{ M}$), it might be $\sim 1.7 \times$
531 10^{-7} M s^{-1} . This value is smaller than that estimated for the SRNOM_{3h} solution, and several
532 explanations of this difference can be proposed: (i) SRNOM_{3h} was a much more complex
533 system than H₂O₂ + acetone and quantitative results cannot be directly transferable;
534 furthermore, calculation lays on an hypothetical value of the bimolecular reaction rate
535 constant of SRNOM_{3h} with •OH; (ii) Acetone was chosen as a model compound but among
536 the carbonyls formed in SRNOM_{3h}, some may absorb more than acetone, especially those
537 bearing double bonds, and/or photodissociate much more easily [Anpo and Kubokawa, 1977];
538 (iii) SRNOM_{3h} also contained chemicals acting probably as better H-donors than acetone and
539 glyphosate, which should favour process 11 and thus the formation of unstable
540 hydroperoxides; (iv) Oxidant species other than •OH might contribute to the photodegradation
541 of glyphosate.

542 In the case of SRNOM, R_{Gly} was much higher than $R_{\text{Gly}}^{\text{H}_2\text{O}_2}$ as for SRNOM_{3h}
543 suggesting that chain reactions might take place as for SRNOM_{3H}, although leading to a much
544 slower production of •OH. Accordingly, the 6-times less formation of ROOR+ROOH from
545 SRNOM than from SRNOM_{3h} suggests that unstable hydroperoxides should be produced in
546 smaller amounts by SRNOM than by SRNOM_{3h}. Spectral measurements showed that
547 SRNOM is much more aromatic than SRNOM_{3h} which constitutes an important difference in
548 terms of •OH reactions. The •OH radicals are known to add on phenols [Lundquist and
549 Eriksson, 2000] to finally produce unreactive phenoxyl radicals while they generate radicals
550 oxidable into hydroperoxides when they abstract hydrogen atoms from aliphatic compounds.
551 Hence, the presence of carbonyls in SRNOM_{3h} could not only favour the formation of radicals
552 through their photolysis but also constitutes a pool of aliphatic compounds oxidable into
553 hydroperoxides.

554 AMPA was the main glyphosate photoproduct detected by UHPLC-HRMS (Figure
555 4B). In the literature, other oxidation products were also detected such as sarcosine [Chen et
556 al, 2007], not detected in this work. After 30 min of irradiation, the highest yield of AMPA
557 was measured with H₂O₂ (66%), followed by SRNOM_{3h} (62%), acetone (57%) and pyruvic
558 acid (38%). Interestingly, when 2-propanol was added to acetone and pyruvate solutions, the
559 yield of AMPA dropped to 10% and 17%, respectively. The formation of AMPA may be thus
560 an indirect evidence of the involvement of •OH radicals in the photodegradation.

561

562 **5. Effect of SRNOM pre-irradiation on •OH, ¹O₂ and ³SRNOM* formation under** 563 **simulated solar light**

564 We also compared the ability of SRNOM and SRNOM_{3h} to photoproduce
565 photooxidants ³SRNOM*, ¹O₂ and •OH in simulated solar-light. After the normalization for
566 light absorption, the rate of 2,4,6-trimethylphenol was found to be 1.5 times higher in SRNOM
567 than in SRNOM_{3h}, in accordance with lower rate of ³SRNOM* formation. Therefore,
568 chromophores yielding ³SRNOM* were partly degraded under UVC irradiation. In the case of
569 ¹O₂ titrated using furfuryl alcohol, we found rates of formation varying by less than 10%
570 between SRNOM and SRNOM_{3h}. At last, results on terephthalic acid used to estimate the rate
571 of •OH formation showed a higher rate of •OH formation in SRNOM_{3h} solution than in
572 SRNOM solution. Taking $k_{\text{SRNOM}} = 1.6 \times 10^8 \text{ M}_C^{-1} \text{ s}^{-1}$ and $k_{\text{SRNOM}_{3h}} = 0.7 \times 10^8 \text{ M}_C^{-1} \text{ s}^{-1}$ for the
573 bimolecular rate constants of reaction with •OH, we got a rate of •OH formation higher by
574 40% for SRNOM_{3h} solution than for SRNOM solution. This enhancement was much lower
575 than the one observed at 254 nm with glyphosate. The dependence of the •OH formation
576 enhancement on the irradiation wavelength supports the hypothesis of the involvement of
577 poorly conjugated and light absorbing carbonyl compounds in the photochemical production
578 of •OH.

579

580 **Conclusion**

581 This work aimed to investigate the effect of UVC irradiation on the ability of SRNOM to
582 generate oxidant species, in particular •OH radicals under UVC. Through in-depth analytical
583 and kinetic studies, we demonstrated that SRNOM irradiation drastically increased the pool of
584 aliphatic carbonyls together with its capacity of photoinducing the degradation of glyphosate
585 at 254 nm. Several experimental results suggest that •OH radicals contributed to this
586 degradation. To better understand the role of carbonyls in the reaction, we studied the
587 photodegradation of glyphosate in the presence of acetone and pyruvate. Experimental data
588 were explained by a mechanism involving a chain reaction in which •OH radicals may be
589 formed through the spontaneous decomposition of unstable hydroperoxides. The same
590 mechanism might prevail in pre-irradiated SRNOM and explain its high efficiency to
591 photodegrade glyphosate upon irradiation at 254 nm. These results show that in UVC
592 treatments NOM could favour the degradation of micropollutants through its high capacity to
593 generate very oxidant radicals. Such a pretreatment of NOM would deserve to be further
594 studied in combination with other engineered water treatment systems.

595

596

597 **Acknowledgments:**

598 This paper is part of a project that received funding from the European Union's Horizon 2020
599 research and innovation programme under the Marie Skłodowska-Curie grant agreement no.
600 765860 (Aquality). The authors would like to thank Martin Lereboure (Engineer CNRS)
601 and Frédéric Emmenegger (Tech CNRS) for UHPLC-MS analyses and Lawrence Frezet
602 (Engineer CNRS) for ESR experiments.

603

604

605

References

606

607 Agbaba, J., Jazic, J.M., Tubic, A., Watson M., Maletić S., Kragulj Isakovski M., Dalmacija B.
608 (2016) Oxidation of natural organic matter with processes involving O₃, H₂O₂ and UV light:
609 formation of oxidation and disinfection by-products. RSC Adv. 6, 86212-86219.

610 DOI:10.1039/C6RA18072H

611

612 Aguer, J. P., Richard, C. (1999) Influence of the excitation wavelength on the photoinductive
613 properties of humic substances. Chemosphere 38, 2293-2301.

614 DOI:10.1016/S0045-6535(98)00447-0

615

616 Anpo, M., Kubokawa, Y. (1977) Reactivity of excited triplet alkyl ketones in
617 solution. I. Quenching and hydrogen abstraction of triplet acetone.

618 Bull. Chem. Soc. Jpn. 1977, 50, 1913.

619 DOI : 10.1246/bcsj.50.1913

620

621 Badali, K. M., Zhou, S., Aljawhary, D., Antiñolo, M., Chen, W. J., Lok, A., Mungall, E.,
622 Wong, J. P. S., Zhao, R., Abbatt, J. P. D. (2015) Formation of hydroxyl radicals from
623 photolysis of secondary organic aerosol material. Atmos. Chem. Phys. 15, 7831–7840.

624 DOI : 10.5194/acp-15-7831-2015

625

626 Brinkmann, T., Horsch, P., Sartorius, D., Frimmel, F. H. (2003) Photoformation of low
627 molecular weight organic acids from brown water dissolved organic matter. Environ. Sci.

628 Technol. 37, 4190-4198.

629 DOI:10.1021/es0263339

630

631 Buchanan, W., Roddick, F., Porter, N. (2016) Formation of Hazardous By-Products Resulting
632 from the Irradiation of Natural Organic Matter: Comparison between UV and VUV
633 Irradiation. *Chemosphere* 63 (7), 1130–1141.

634 DOI:10.1016/j.chemosphere.2005.09.040.

635

636 Buxton, G. V. , Greenstock, C.L. , Helman, W. P. , Ross, A. B. (1988) Critical review of rate
637 constants fro reactions of hydrated electrons, hydrogen atoms and hydroxyl radicas in aqueous
638 solution. *J. Phys. Chem. Ref. Data* 17, 513-886.

639 DOI:10.1063/1.555805

640

641 Chen, Y., Wu, F., Lin, Y., Deng, N., Bazhin, N., Glebov, E. (2007) Photodegradation of
642 glyphosate in the ferrioxalate system. *J. Hazard. Mat.* 148, 360–365.

643 DOI : 10.1016/j.jhazmat.2007.02.044

644

645 Corin, N., Backlund, P., Kulovaara, M. (1996) Degradation products formed during UV-
646 irradiation of humic waters. *Chemosphere* 33, 245-255.

647 DOI:10.1016/0045-6535(96)00167-1

648

649 de Bryun, W.J., Clark, C.D., Pagel, L., Takehara, C. (2011) Photochemical production of
650 formaldehyde, acetaldehyde and acetone from chromophoric dissolved organic matter in
651 coastal waters. *J Photochem Photobiol A*, 226, 16-22.

652 DOI:10.1016/j.jphotochem.2011.10.002

653

654 Dong, M. M., Rosario-Ortiz, F. L. (2012) Photochemical formation of hydroxyl radical from
655 effluent organic matter. *Environ. Sci. Technol.* 46, 3788-3794.
656 DOI : 10.1021/es2043454
657
658 Fukushima, M., Tatsumi, K. (2001) Degradation characteristics of humic acid during photo-
659 fenton processes. *Environ. Sci. Technol.* 35, 3683-3690.
660 DOI:10.1021/es0018825
661
662 Gan, D., Jia, M., Vaughan, P. P., Falvey, D. E., Blough, N. V. (2008) Aqueous
663 Photochemistry of Methyl-Benzoquinone *J. Phys. Chem. A* 112, 2803– 2812.
664 DOI: 10.1021/jp710724e
665
666 Garg, S., Rose, A. L., Waite, T. D. (2011) Photochemical production of superoxide and
667 hydrogen peroxide from natural organic matter *Geochim. Cosmochim. Acta* 75, 4310-4320.
668 DOI : 10.1016/j.gca.2011.05.014
669
670 Goldstone, J.V., Pullin, M.J., Bertilsson, S., Voelker, B.M. (2002) Reactions of hydroxyl
671 radicals with humic substances : bleaching, mineralization and production of bioavailable
672 carbon substrates. *Environ. Sci. Technol.* 36, 364-372.
673 DOI:10.1021/es0109646
674
675 Hao, W., Zhanghao, C., Feng, S., Jingyi, L., Xin, J., Chao, W., Cheng G. (2020)
676 Characterization for the transformation of dissolved organic matters during ultraviolet
677 disinfection by differential absorbance spectroscopy. *Chemosphere* 243, 125374.
678 DOI:10.1016/j.chemosphere.2019.125374

679

680 Ike, I. A., Karanfil, T., Cho, J., Hur J. (2019) Oxidation byproducts from the degradation of
681 dissolved organic matter by advanced oxidation processes -A critical review
682 Water Res. 164 114929.
683 DOI:10.1016/j.watres.2019.114929
684

685 Kieber, R.J., Zhou, X., Mopper, K. (1990) Formation of carbonyl compounds from UV-
686 induced photodegradation of humic substances in natural waters : fate of riverine carbon in
687 the sea. Limnol. Oceanogr. 35, 1503-1515.
688 DOI:10.4319/lo.1990.35.7.1503
689

690 Krapf, M., Haddad, I. E., Bruns, E. A., Molteni, U., Daellenbach, K. R., Prevot, A. S. H.,
691 Baltensperger, U., Dommen, J. (2016) Labile Peroxides in Secondary Organic Aerosol.
692 Chem 1, 603–616.
693 DOI : 10.1016/j.chempr.2016.09.007
694

695 Kulovaara, M., Corin, N., Backlund, P., Tervo J. (1996) Impact of UV₂₅₄-irradiation on
696 aquatic humic substances. Chemosphere 33, 783-790.
697 DOI:10.1016/0045-6535(96)00233-0
698

699 Lamsal, R., Walsh, M. E., Gagnon, G. A. (2011) Comparison of advanced oxidation processes
700 for the removal of natural organic matter. Water Res. 45, 3263-3269.
701 DOI:10.1016/j.watres.2011.03.038
702

703 Leresche, F., McKay, G., Kurtz, T., von Gunten, U., Canonica, S., Rosario-Ortiz, F. L. (2019)

704 Effects of Ozone on the Photochemical and Photophysical Properties of Dissolved Organic
705 Matter. *Environ. Sci. Technol.* 53, 5622–5632.
706 DOI: 10.1021/acs.est.8b06410
707
708 Lester, Y., Sharpless, C. M., Mamane, H., Linden, K. G. (2013) Production of Photo-oxidants
709 by Dissolved Organic Matter During UV Water Treatment. *Environ. Sci. Technol.* 47,
710 11726–11733.
711 DOI : 10.1021/es402879x
712
713 Lundqvist, M. J., Eriksson, L. A. (2000) Hydroxyl Radical Reactions with Phenol as a Model
714 for Generation of Biologically Reactive Tyrosyl Radicals. *J. Phys. Chem. B* 104, 848-855.
715 DOI : 10.1021/jp993011r
716
717 McKay, G., Rosario-Ortiz, F. L. (2015) Temperature Dependence of the Photochemical
718 Formation of Hydroxyl Radical from Dissolved Organic Matter *Environ. Sci. Technol.* 49,
719 4147– 4154.
720 DOI: 10.1021/acs.est.5b00102
721
722 Miller, W.L., Kester, D.R. (1988) Hydrogen peroxide measurement in seawater by (p-
723 hydroxyphenyl) acetic acid dimerization. *Anal. Chem.* 60, 2711-2715.
724 DOI:10.1021/ac00175a014
725
726 Mostafa, S., Rosario-Ortiz, F. L. (2013) Singlet Oxygen Formation from Wastewater Organic
727 Matter. *Environ. Sci. Technol.* 47, 8179–8186.
728 DOI:10.1021/es401814s

729

730 Page, S. E., Arnold, W. A., McNeill, K. (2011) Assessing the Contribution of Free Hydroxyl
731 Radical in Organic Matter-Sensitized Photohydroxylation Reactions Environ. Sci. Technol.
732 45, 2818– 2825.

733 DOI: 10.1021/es2000694

734

735 Palma, D., Sleiman, M., Voldoire, O. et al. Study of the dissolved organic matter (DOM) of
736 the Auzon cut-off meander (Allier River, France) by spectral and photoreactivity approaches.
737 Environ Sci Pollut Res 27, 26385–26394 (2020).

738 DOI: 10.1007/s11356-020-09005-7

739

740 Patel-Sorrentino, N., Mounier, S., Lucas, Y., Benaim, J.Y. (2004) Effects of UV–visible
741 irradiation on natural organic matter from the Amazon basin. Sci. Tot. Environ. 321, 231-239

742 DOI:10.1016/j.scitotenv.2003.08.017

743

744 Paul, A., Dziallas, C., Zwirnmann, E., Gjessing, E.T., Grossart, H.P. (2012) UV irradiation of
745 natural organic matter (NOM): impact on organic carbon and bacteria. Aquatic Sciences
746 74, 443–454.

747 DOI:10.1007/s00027-011-0239-y

748

749 Pearson, G. S. (1963) The photooxidation of acetone. J. Chem. Phys. 67, 1686-1692.

750 DOI: 10.1021/j100802a026

751

752 Polewski, K., Slawinska, D., Slawinski, J , Pawlak, A. (2005) The effect of UV and visible
753 light radiation on natural humic acid and EPR spectral and kinetic studies. *Geoderma* 126,
754 291-299.
755 DOI:10.1016/j.geoderma.2004.10.001
756
757 Rosario-Ortiz, F.L., Canonica, S. (2016) Probe Compounds to Assess the Photochemical
758 Activity of Dissolved Organic Matter. *Environ Sci Technol* 50, 12532–12547.
759 DOI:10.1021/acs.est.6b02776
760
761 Rougé, V., von Gunten, U., Lafont de Sentenac, M., Massi, M., Wright, P. J., Croué, J. P.,
762 Allard, S. (2021). Comparison of the impact of ozone, chlorine dioxide, ferrate and
763 permanganate pre-oxidation on organic disinfection byproduct formation during post-
764 chlorination *Environ. Sci.: Water Res. Technol.* 6, 2382-2395.
765 DOI : 10.1039/D0EW00411A
766
767 Sarathy, S. R., Stefan, M. I., Royce, A., Mohseni, M. (2011) Pilot-scale UV/H₂O₂ advanced
768 oxidation process for surface water treatment and downstream biological treatment: effects on
769 natural organic matter characteristics and DBP formation potential.
770 *Environ. Technol.* 32, 1709-1718.
771 DOI:10.1080/09593330.2011.553843
772
773 Sarathy, S. R., Mohseni M. (2007) The Impact of UV/H₂O₂ Advanced Oxidation on
774 Molecular Size Distribution of Chromophoric Natural Organic Matter.
775 *Environ. Sci. Technol.* 41, 8315-8320.
776 DOI:10.1021/es071602m

777

778 Sarathy, S. R., Stefan, M. I., Royce, A., Mohseni, M. (2011) Pilot-scale UV/H₂O₂ advanced
779 oxidation process for surface water treatment and downstream biological treatment: effects on
780 natural organic matter characteristics and DBP formation potential.
781 Environ. Technol. 32, 1709-1718.
782 DOI:10.1080/09593330.2011.553843

783

784 Schmitt-Kopplin, P., Hertkorn, N., Schulten, H. R., Kettrup, A. (1998) Structural Changes in
785 a Dissolved Soil Humic Acid during Photochemical Degradation Processes under O₂ and N₂
786 Atmosphere. Environ. Sci. Technol. 32, 2531-2541.
787 DOI:10.1021/es970636z

788

789 Sillanpää, M., ChakerNcibi, M., Matilainen, A. (2018) Advanced oxidation processes for the
790 removal of natural organic matter from drinking water sources: A comprehensive review
791 J Environ. Manag. 208 56-76.
792 DOI:10.1016/j.jenvman.2017.12.009

793

794 Soman, A., Qiu, Y., Chan Li, Q. (2008) HPLC-UV Method Development and Validation for
795 the Determination of Low Level Formaldehyde in a drug Substance. J. Chromatog. Sci. 46
796 461-465.
797 DOI:0.1093/chromsci/46.6.461

798

799 Stefan, M. , Hoy, A., Bolton, J.R. (1996) Kinetics and Mechanism of the Degradation and
800 Mineralization of Acetone in Dilute Aqueous Solution Sensitized by the UV Photolysis of
801 Hydrogen Peroxide. Environ. Sci. Technol. 30, 2382-2390.

802 DOI : 10.1021/es950866i

803

804 Stefan, M. I., Bolton, J. R. (1999) Reinvestigation of the Acetone Degradation Mechanism in

805 Dilute Aqueous Solution by the UV/H₂O₂ Process. *Environ. Sci. Technol.* 33, 6, 870–873

806 DOI : 10.1021/es9808548

807

808 Sun, L., Qian, J., Blough, N. V., Mopper, K. Insights into the Photoproduction Sites of

809 Hydroxyl Radicals by Dissolved Organic Matter in Natural Waters *Environ. Sci. Technol.*

810 *Lett.* **2015**, 2 (12) 352– 356.

811 DOI: 10.1021/acs.estlett.5b00294

812

813 Sun, Q., Ma, J., Yan, S., Song, W. (2021). Photochemical formation of methylhydroperoxide

814 in dissolved organic matter solutions. *Env. Sci. Technol.* 52, 1076-1087.

815 DOI: 10.1021/acs.est0c07717

816

817 Tafer, R., Sleiman, M., Boulkamh, A., Richard, C. (2016) Photomineralization of aqueous

818 salicylic acids. Photoproducts characterization and formation of light induced secondary OH

819 precursors (LIS-OH). *Water Res.* 106, 496-506.

820 DOI : 10.1016/j.watres.2016.10.038

821

822 Tang, W.W., Zeng, G.M., Gong, J.-L., Liang, J., Xu, P., Zhang, C., Huang, B.-B. (2014)

823 Impact of Humic/Fulvic Acid on the Removal of Heavy Metals from Aqueous Solutions

824 Using Nanomaterials: A Review. *Sci. Total Environ.* 468–469, 1014–1027.

825 DOI:10.1016/j.scitotenv.2013.09.044.

826

827 Thomson, J., Roddick, F.A., Drikas, M. (2004) Vacuum ultraviolet irradiation for natural
828 organic matter removal. *J. Water Supply Res. Technol. - Aqua* 53 193-206.
829 DOI:10.2166/aqua.2004.0017
830
831 Varanasi, L., Coscarelli, E., Khaksari, M., Mazzoleni, L. R., Minakata, D. (2018)
832 Transformations of dissolved organic matter induced by UV photolysis, Hydroxyl radicals,
833 chlorine radicals, and sulfate radicals in aqueous-phase UV-Based advanced oxidation
834 processes. *Water Res.* 135, 22-30.
835 DOI:10.1016/j.watres.2018.02.015
836
837 Vaughan, P. P., Blough, N. V. (1998) Photochemical formation of hydroxyl radical by
838 constituents of natural waters. *Environ. Sci. Technol.* 32, 2947-2953.
839 DOI :10.1021/es9710417
840
841 Vidal, E., Negro, A., Cassano, A., Zalazar, C. (2015) Simplified reaction kinetics, models and
842 experiments for glyphosate degradation in water by the UV/H₂O₂ process.
843 *Photochem Photobiol Sci* 14, 366-377.
844 DOI : 10.1039/C4PP00248B
845
846 Vione, D., Minella, M., Maurino, W., Minero, C. 2014. Indirect Photochemistry in Sunlit
847 Surface Waters: Photoinduced Production of Reactive Transient Species. *Chem. Eur. J.* 20,
848 10590 – 10606.
849 DOI: 10.1002/chem.201400413
850

851 Wang, D., Duan, X., He, X., Dionysiou, D. D. (2016) Degradation of dibutyl phthalate (DBP)
852 by UV-254 nm/H₂O₂ photochemical oxidation: kinetics and influence of various process
853 parameters. *Environ Sci Pollut Res Int.* 23, 23772-23780.

854 DOI:10.1007/s11356-016-7569-1

855

856 Weissnar, J., Aiken, G. R., Bergamaschi, B. A., Fram, M. S., Fugii, R., Mopper, K. (2003)
857 Evaluation of specific ultraviolet absorbance as an indicator of the chemical composition and
858 reactivity of dissolved organic carbon. *Environ Sci Technol* 37, 4702–4708.

859 DOI:10.1021/es030360x

860

861 Wenk, J., Aeschbacher, M., Sander, M., von Gunten, U., Canonica, S. (2015) Photosensitizing
862 and inhibitory effects of ozonated dissolved organic matter on triplet-induced contaminant
863 transformation. *Environ. Sci. Technol.* 49, 8541–8549.

864 DOI:10.1021/acs.est.5b02221

865

866 Westerhoff, P., Mezyk, S. P., Cooper, W. J., Minakata, D. (2007) Electron Pulse Radiolysis
867 Determination of Hydroxyl Radical Rate Constants with Suwannee River Fulvic Acid and
868 Other Dissolved Organic Matter Isolates. *Env. Sci Technol* 41, 4640-4640.

869 DOI : 10.1021/es062529n

870

871 Yu, J., Flagan, R., Seinfeld, J. (1998) Identification of Products Containing -COOH, -OH, and
872 -C=O in atmospheric oxidation of hydrocarbons. *Environ. Sci. Technol* 32, 2357-2370.

873 DOI:10.1021/es980129x

874

875 Yu, X. Y., Barker, J. R. (2003) Hydrogen peroxide photolysis in acidic aqueous solutions
876 containing chloride ions. I. Chemical mechanism. *J. Phys. Chem. A*, 107, 9, 1313–1324
877 DOI : 10.1021/jp0266648

878

879 Zhang, S., Rougé, V., Gutierrez, L., Croué, J. P. (2019) Reactivity of chromophoric dissolved
880 organic matter (CDOM) to sulfate radicals: Reaction kinetics and structural transformation
881 *Water Res.* 163, 114846.

882 DOI:10.1016/j.watres.2019.07.013

883

884 Zhong, X., Cui, C., Yu, S. (2017) Identifying oxidation intermediates formed during ozone-
885 UV of fulvic acid. *Desalination and Water Treatment* 74, 258-268.

886 DOI :10.5004/dwt.2017.20587

887

888 Zhou, Y., Cheng, F. , He, D., Zhang, Y., Qua,J. , Yang, X., Chenc, J., Peijnenburg, W. J. G.
889 M. (2021) Effect of UV/chlorine treatment on photophysical and photochemical properties of
890 dissolved organic matter. *Water Res.* 192, 116857.

891 DOI : 10.1016/j.watres.2021.116857

892

893 Zoschke, K., Dietrich, N., Bornick, H., Worch, E. (2012). UV-based advanced oxidation
894 processes for the treatment of odour compounds: efficiency and by-product formation.
895 *Water Res.* 46, 5365-5373.

896 DOI :10.1016/j.watres.2012.07.012

897

898

899